

# Vehicular and Core–Shell Nanoparticle Diffusion in Attractive Entangled Polymer Melts

Kaitlin Wang and Karen I. Winey\*



Cite This: *Macromolecules* 2024, 57, 6789–6795



Read Online

ACCESS |



Metrics & More

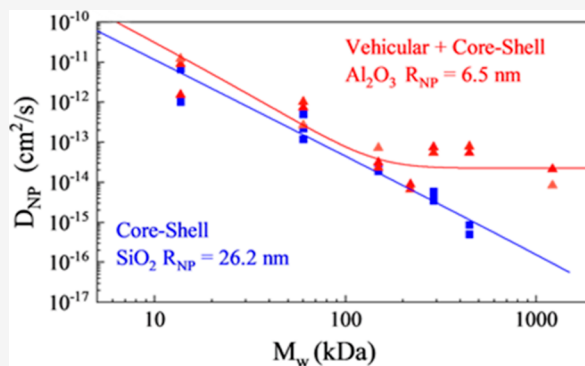


Article Recommendations



Supporting Information

**ABSTRACT:** This work studies nanoparticle (NP) diffusion in attractive polymer melts and reveals two distinct dynamic modes: vehicular and core–shell. By diffusing alumina NPs ( $R_{\text{NP}} = 6.5$  nm) and silica NPs ( $R_{\text{NP}} = 8.3$  and 26.2 nm) into poly(2-vinylpyridine) melts of various molecular weights (14–1220 kDa), we examine the impact of the  $R_{\text{NP}}$ , polymer size ( $R_g$ ), and surface chemistry on NP diffusion. Using time-of-flight secondary ion mass spectrometry and trilayer samples, we measure cross-sectional nanoparticle concentration profiles as a function of the annealing time and extract nanoparticle diffusion coefficients. Both small and large silica NPs ( $R_g/R_{\text{NP}} = 0.12$ –3.6) display core–shell behavior, while alumina NPs ( $R_g/R_{\text{NP}} = 0.50$ –4.6) diverge sharply with increasing polymer molecular weight, aligning with theoretically predicted vehicular diffusion. The transition from core–shell to vehicular diffusion is the result of both increasing molecular weight and weaker NP/polymer attractions and facilitates an estimate of the monomer desorption time.



## INTRODUCTION

Polymer nanocomposites (PNCs) have garnered considerable interest as advanced materials due to their tunable properties. Introducing nanoparticles (NPs) into a polymer matrix permits nuanced adjustments to optimize mechanical, thermal, electrical, and optical attributes to meet specific performance criteria. This adaptability positions PNCs as a promising material class across diverse sectors including electronics, aerospace, automotive, and biomedical industries.<sup>1–4</sup>

Previous work has clearly established that the spatial distribution of NPs significantly impacts processability and properties, including mechanical properties, rheology, and gas permeability within PNCs.<sup>5–8</sup> To achieve and maintain the desired properties, understanding and predicting NP diffusion are critically important. Factors such as NP size, NP shape, NP concentration, and the interaction between polymer and NPs must be managed to achieve desired NP distributions and properties for effective PNC applications.<sup>9–11</sup> PNCs with strong attractions between the NPs and polymer matrix are distinguished by improved NP dispersion and maintain industrially relevant processability advantages compared with their neutral counterparts. Thus, NP diffusion behavior in these attractive nanocomposites is of particular interest and a crucial cornerstone for PNC applications.<sup>12</sup>

When particles are microscopic, particle diffusion in a viscous medium is well described by Stokes–Einstein (SE) behavior,  $D_{\text{SE}} = \frac{k_B T}{6\pi\eta R}$ . However, significant deviations have been reported for NP diffusion, particularly in the presence of

attractive polymer–NP interactions.<sup>13–19</sup> NP diffusion studies in neutral melts have also highlighted substantial deviations from SE, depending on the NP radius and polymer tube diameter,  $d_T$ .<sup>18,20,21</sup> In athermal systems, spherical NPs with diameters larger than  $d_T$  exhibit a hopping diffusion mechanism in which the NPs overcome topological energy barriers to move faster than SE predictions.<sup>22</sup> Small NPs, due to their size being comparable to or smaller than the polymer's mesh size, exhibit diffusion rates largely unaffected by the surrounding polymer.<sup>23</sup> Within attractive melts, Schweizer's group introduced two simultaneous NP diffusion modes—the core–shell and vehicle modes—where the relative time scales of polymer and NP dynamics dictate the dominant mode.<sup>16,17</sup> The total diffusion coefficient of a NP is described by the sum of the core–shell and vehicle modes

$$D_{\text{NP,theory}} = D_{\text{core-shell}} + D_{\text{vehicle}} \quad (1)$$

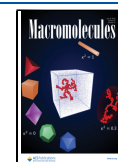
The core–shell contribution follows the SE behavior and accounts for (1) the viscosity of the PNC rather than the neat polymer and (2) the effective NP size rather than the bare NP size due to a bound polymer layer

**Received:** April 9, 2024

**Revised:** June 7, 2024

**Accepted:** June 21, 2024

**Published:** July 8, 2024



$$D_{\text{core-shell}} = \frac{k_B T}{6\pi\eta_{\text{PNC}}R_{\text{eff}}} \quad (2)$$

where  $k_B$  is the Boltzmann constant,  $T$  is the annealing temperature in Kelvin,  $\eta_{\text{PNC}}$  is the PNC viscosity in Pa·s, and the effective NP radius is  $R_{\text{eff}} = R_{\text{NP}} + R_g$ . These modifications to the SE behavior result in slower NP diffusion. A variety of experimental methods have been used to measure diffusion coefficients of NPs in polymer melts, including Rutherford backscattering (RBS) ( $R_{\text{NP}} = 13$  nm),<sup>14,24</sup> dynamic light scattering (DLS) ( $R_{\text{NP}} = 0.88$ , 5 nm),<sup>17</sup> and single particle tracking (SPT) ( $R_{\text{NP}} = 6.5$ – $6.6$  nm).<sup>25</sup> The core-shell mechanism (eq 2) alone has been sufficient to understand NP diffusion in various experimental systems with strong polymer–NP interactions: unentangled poly(propylene glycol) (PPG) melts with octaamino-phenylsilsequioxane (OAPS) NPs,<sup>17</sup> PPG with small silica (SiO<sub>2</sub>) NPs,<sup>17</sup> and poly(2-vinylpyridine) (P2VP) with SiO<sub>2</sub> NPs.<sup>14</sup> In addition, there are examples of  $D_{\text{NP}} < D_{\text{SE}}$  in poly(ethylene oxide) with SiO<sub>2</sub> NPs<sup>26</sup> and PPG with strongly interacting quantum dot samples through COOH surface functionalization.<sup>27</sup> These systems represent a wide range of  $R_g/R_{\text{NP}}$  ( $\sim 0.1$ – $1.2$ ), and the core-shell model explains well the decrease in  $D_{\text{NP}}$  compared to SE behavior.

The vehicular mode for NP diffusion involves polymer desorption and results in diffusion coefficients faster than SE behavior when the desorption of the polymer is faster than the polymer chain dynamics. This mechanism is described by using four polymer time scales:  $\tau_{\text{des}}$ —monomer desorption time,  $\tau_e$ —entanglement onset time,  $\tau_{\text{Rouse}}$ —longest chain Rouse relaxation time, and  $\tau_{\text{rep}}$ —reptation time.<sup>16</sup> In Regime I, the monomer desorption time is relatively quick, meaning shorter than the entanglement onset time ( $\tau_{\text{des}} < \tau_e$ ). In this regime, the vehicular contribution to  $D_{\text{NP,theory}}$  scales as  $\sim \tau_{\text{des}}^{-1}$  as

$$D_{\text{vehicle-I}} = Ab \times \frac{D_0}{\tau_{\text{des}}} \quad (3)$$

where  $A$  is a numerical prefactor,  $b$  is the Kuhn monomer length, and  $D_0$  is the segmental diffusion constant. In this study, Regime I will be neglected because the NPs have surface hydroxyl groups that interact favorably with the polymer, such that  $\tau_{\text{des}}$  is expected to be longer than  $\tau_e$ . In Regime II, the desorption time is longer than the entanglement onset time and shorter than the Rouse time ( $\tau_e < \tau_{\text{des}} < \tau_{\text{Rouse}}$ ), indicating an intermediately strong NP–polymer attraction, such that the vehicular contribution to NP diffusion scales  $\sim 1/\tau_{\text{des}}^{3/4}$  as

$$D_{\text{vehicle-II}} = Ad_T(b^2D_0)^{1/4} \times \left(\frac{1}{\tau_{\text{des}}}\right)^{3/4} \quad (4)$$

where  $d_T$  is the tube diameter. At slower desorption times, although still faster than polymer reptation ( $\tau_R < \tau_{\text{des}} < \tau_{\text{rep}}$ ), the vehicular contribution to NP diffusion in Regime III has a molecular weight dependence

$$D_{\text{vehicle-III}} = Ad_T \left(\frac{D_0}{N\tau_{\text{des}}}\right)^{1/2} \quad (5)$$

where  $N$  is the degree of polymerization. Regime III is the only case in which  $D_{\text{vehicle}}$  depends on both desorption time and the polymer molecular weight with a scaling dependence of  $(N\tau_{\text{des}})^{-1/2}$ . To date, the experimental systems that suggest a

vehicular mechanism for NP diffusion have used very small NPs ( $R_{\text{NP}} < 1$  nm). Specifically, nanocomposites of PPG with OAPS and P2VP with OAPS exhibit fast NP diffusion relative to the core-shell model.<sup>13,17</sup>

In this article, we experimentally identify PNCs with NP diffusion controlled by both core-shell and the vehicular modes. Leveraging the capabilities of our previously demonstrated time-of-flight secondary ion mass spectrometry (ToF-SIMS) method,<sup>28</sup> we accurately measure NP diffusion coefficients on micron length scales and across a considerable range,  $D_{\text{NP}} = 10^{-18}$  to  $10^{-11}$  cm<sup>2</sup>/s. By employing a wide range of P2VP molecular weights (14–1220 kg/mol) and three NPs that vary in size and surface chemistry, we reveal systems dominated by core-shell and vehicle NP diffusion. Finally, we discuss the implications of these distinct diffusion modes and estimate desorption times ( $\tau_{\text{des}}$ ) of the bound layer.

**Experimental Methods. Materials.** P2VP of weight-averaged molecular weights 14.0, 41.0, 158, 219, 310, 474, and 1220 kDa (narrow distribution, PDI < 1.10) was purchased from Scientific Polymer Products Inc. and used as received. Gel permeation chromatography (GPC) was used to measure the polymers' molecular weights and respective PDIs (Table S1). Nissan-STL SiO<sub>2</sub> NPs were solvent exchanged from methyl-ethyl ketone (MEK) to methanol (MeOH) via crashing the particles out of MEK.<sup>28</sup> Aluminum oxide (Al<sub>2</sub>O<sub>3</sub>) NPs were purchased from Sigma-Aldrich, then suspended in a 50 g/L MeOH solution, vortexed for 1 min, sonicated for >30 min, and filtered through 1 and 0.2  $\mu\text{m}$  filters subsequently. A small amount of the respective molecular weight of P2VP (5 g/L) was added to the MeOH–Al<sub>2</sub>O<sub>3</sub> solution to form a bound layer on the bare NPs to prevent subsequent aggregation. The solution was stirred constantly, and excess MeOH was evaporated to achieve the desired NP vol % after filtration. Ludox SiO<sub>2</sub> NPs were solvent exchanged from water to ethanol through creating a miscible water/ethanol solution, then adding concentrated P2VP/ethanol solution. The solution was then diluted with ethanol to the desired concentration. NP sizes and size dispersities were determined using small-angle X-ray scattering (SAXS) on a capillary filled with a dilute NP suspension and fit using the hard sphere model. The Nissan SiO<sub>2</sub> NPs fit to a hard sphere resulted in  $R_{\text{NP}} = 26.1$  nm, PDI 1.19, and the Ludox SiO<sub>2</sub> NPs measured  $R_{\text{NP}} = 8.3$  nm and PDI = 1.15. Aluminum oxide (Al<sub>2</sub>O<sub>3</sub>) NPs measured  $R_{\text{NP}} = 6.5 \pm 2.5$  nm and PDI = 1.14, with DLS measuring hydrodynamic diameter consistent with  $\sim R_{\text{NP}} + R_g$ . Silicon wafers (<100>) with a thick thermal oxide layer (referred to as SiO<sub>2</sub> wafers hereafter) were purchased from Nova Electronic Materials. Silicon wafers (<100>) (Si wafer) were purchased from Wafer World Inc.

**Trilayer Fabrication and NP Diffusion.** Building upon our earlier study,<sup>28</sup> we crafted trilayer samples composed of a thin PNC layer placed between two thick P2VP matrix layers. Upon annealing, NPs diffuse into the homopolymer layers and we measure the NP tracer diffusion coefficient,  $D_{\text{NP}}$ .<sup>28</sup> The P2VP matrix films were prepared via spin coating; the P2VP base layer was created by spin coating a viscous P2VP-methanol (MeOH) solution at 1000–2000 rpm for 1 min onto Si wafers to achieve a  $\sim 4$   $\mu\text{m}$  matrix film. To prepare the PNC midlayers, 10 vol % SiO<sub>2</sub> NP or 5 vol % Al<sub>2</sub>O<sub>3</sub> NP was suspended in P2VP MeOH solutions of varying concentrations and spin-coated onto SiO<sub>2</sub> wafers at 1000–2000 rpm for 1 min to achieve a thickness of  $200 \pm 60$  nm. PNC layer thicknesses were measured via scanning electron microscopy (SEM), and

the thickness was averaged over two samples. The P2VP top layers were spin-coated from varying concentrations of P2VP solutions onto SiO<sub>2</sub> wafers (~4 μm). Specific solution concentrations and spin-coating conditions for each layer are listed in Tables S2 and S3. Similar to our previous report,<sup>28</sup> each PNC layer was transferred to a P2VP base layer by etching the spun coat PNC layer off the SiO<sub>2</sub> wafer using a 20 wt % NaOH solution, resulting in a floating PNC film that can be rinsed with DI water and stacked on top of the P2VP base layer. The top P2VP layer was transferred to the bilayer similarly. Each trilayer specimen was annealed in a specialized custom-built oven, precisely set at 180 °C under vacuum conditions (<50 Pa) for durations spanning from 10 min to 10 days. Annealing times were selected to achieve diffusion distances of ~0.5–3 μm.

**Preparing Trilayer Samples for ToF-SIMS.** To obtain the cross-sectional view, a diamond scribe was used to fracture samples along a crystallographic plane of the silicon wafer to preserve the polymer/wafer interface. Samples were cleaned with a nitrogen gas gun to remove SiO<sub>2</sub> dust on the surface. Carbon paint suspended in MEK was applied across the back of the wafer to reduce surface charging and improve the ion yield.

**ToF-SIMS.** Time-of-flight secondary ion mass spectrometry is a powerful surface analysis technique that provides 3D compositional information. In ToF-SIMS, a focused beam of high-energy ions sputters molecular fragments from the material and a mass spectrometer analyzes the resulting secondary ions to determine their mass-to-charge ratio, resulting in a 2D compositional map as each layer is removed.<sup>29</sup> ToF-SIMS has a wide range of applications in polymer science, particularly for the analysis of surface and interface properties of polymers and polymer composites.<sup>30–33</sup> Our previous work produced accurate SiO<sub>2</sub> NP and polystyrene diffusion coefficients and established ToF-SIMS as a powerful technique to measure both polymer and NP diffusion given that the diffusing species produce ions that are distinct from the background matrix.<sup>28</sup>

ToF-SIMS measurements were performed using a TESCAN S8252X dual-beam plasma FIB-SEM with Xe<sup>+</sup>. Unless otherwise noted, measurements were taken with Xe<sup>+</sup> FIB parameters at 30 keV and 100 pA with 1024 × 1024 pixel resolution on positive ion mode for 300 (SiO<sub>2</sub> NPs) or 400 frames (Al<sub>2</sub>O<sub>3</sub> NPs). Additional frames were collected for the Al<sub>2</sub>O<sub>3</sub> NPs to improve the signal due to the lower NP loading (5 vol %) present. A 20 × 20 μm<sup>2</sup> field of view (FoV) was used during collection, and the ToF-SIMS images were produced using a 2 × 2 bin width, resulting in a 512 × 512-pixel image.

NP diffusion coefficients were determined by allowing NPs to travel for a set time ( $t = 10$  min–10 days) at a chosen temperature ( $T = 180$  °C) and measuring the corresponding NP concentration profiles using ToF-SIMS. Cross-sectioned trilayer samples were measured by scanning across the P2VP/PNC/P2VP interfaces using the Xe<sup>+</sup> beam, which produces the 3D ion intensity map for each mass/charge ( $m/q$ ) value. To detect the SiO<sub>2</sub> and Al<sub>2</sub>O<sub>3</sub> NP concentrations, we use  $m/q = 28$  and 27, respectively (Figure S1). 1D concentration profiles were extracted from the 3D data set by integrating along the  $x$  and  $z$  directions after tilting the data set to align the plane of the highest NP concentration within the sample to  $y = 0$ .<sup>28</sup> We then deconvoluted the beam resolution function (Gaussian with fwhm = 0.2 μm) from the raw concentration profile to obtain the ion concentration profile. This 1D concentration

profile was iteratively fit to Fick's second law for a finite source diffusing into a semi-infinite medium using

$$\varphi(y) = \frac{1}{2} \left[ \operatorname{erf} \left( \frac{h-y}{\sqrt{4D_{\text{NP}}t}} \right) + \operatorname{erf} \left( \frac{h+y}{\sqrt{4D_{\text{NP}}t}} \right) \right] \quad (6)$$

where  $\varphi(y)$  is the NP concentration as a function of position  $y$ ,  $h$  is the initial thickness of the PNC layer,  $t$  is time in seconds, and  $D_{\text{NP}}$  is the NP diffusion coefficient. By this process, we determine  $D_{\text{NP}}$  as demonstrated in our prior work.<sup>28</sup>

## RESULTS AND DISCUSSION

**NP Diffusion Coefficients as a Function of Molecular Weight.** We measured NP diffusion into P2VP matrices of molecular weights from 14 to 1220 kDa using our ToF-SIMS method to measure NP diffusion coefficients,  $D_{\text{NP}}$ , in entangled polymer melts. We obtain diffusion coefficients after annealing for two or three annealing times to demonstrate that the NP tracer diffusion is independent of the annealing time. We employ the radius of gyration ( $R_g$ ) as a metric for polymer size. Figure 1 shows representative SiO<sub>2</sub> ( $R_{\text{NP}} = 26.2$  nm) and Al<sub>2</sub>O<sub>3</sub> ( $R_{\text{NP}} = 6.5$  nm) NP concentration profiles after various annealing times at 180 °C in 41 kDa P2VP ( $R_g = 5.5$  nm) along with fits to eq 6 to obtain the diffusion coefficients. In this  $R_g < R_{\text{NP}}$  regime ( $d_T = 23.5$  nm), the smaller Al<sub>2</sub>O<sub>3</sub> NPs diffuse faster than the larger SiO<sub>2</sub> NPs and the results are consistent with  $D_{\text{core-shell}}$  (eq 2). Specifically,  $\langle D_{\text{NP}}(\text{SiO}_2, 26.2 \text{ nm}) \rangle = 2.8 \pm 2.0 \times 10^{-13}$  cm<sup>2</sup>/s and  $D_{\text{core-shell}}$  for this system is  $3.1 \times 10^{-13}$  cm<sup>2</sup>/s and  $\langle D_{\text{NP}}(\text{Al}_2\text{O}_3, 6.5 \text{ nm}) \rangle = 7.4 \pm 2.5 \times 10^{-13}$  cm<sup>2</sup>/s and  $D_{\text{core-shell}}$  for this system is  $9.0 \times 10^{-13}$  cm<sup>2</sup>/s. Fitting the NP concentration profiles is repeated in six other molecular weights and allows us to obtain diffusion coefficients across orders of magnitude by adjusting the annealing time. The experimental concentration profiles for all NP/P2VP systems and their respective fits are given in Figures S2–S4, with tabulated data in Tables S4–S6. While most of the systems studied found  $D_{\text{NP}} \approx D_{\text{core-shell}}$ , we also found systems where  $D_{\text{NP}} > D_{\text{core-shell}}$  indicating the presence of a vehicular mechanism of NP diffusion in entangled polymer melts.

**Core-Shell and Vehicle Diffusion Behavior.** In contrast to our earlier experimental investigations, this study involves P2VP matrices spanning a wider molecular weight range of 14–1220 kDa, which includes unentangled to well-entangled ( $M_e \approx 18$  kDa) polymer melts. To accommodate the high viscosity matrices, diffusion times were carefully controlled from 10 min to 10 days to achieve diffusion lengths commensurate with ToF-SIMS measurements. Thus, we measure  $D_{\text{NP}}$  values ranging from  $7 \times 10^{-18}$  to  $1.3 \times 10^{-11}$  cm<sup>2</sup>/s, which is sufficient to capture both core-shell and vehicular NP diffusion mechanism.

The larger SiO<sub>2</sub> NPs ( $R_{\text{NP}} = 26$  nm) clearly exhibit core-shell model behavior across the entire molecular weight range. In Figure 2, the  $D_{\text{NP}}$  values from the different annealing times are normalized by  $D_{\text{core-shell}}$  (eq 2) and the values are on the order of 1. Similarly, the diffusion coefficients for smaller SiO<sub>2</sub> NPs ( $R_{\text{NP}} = 8.3$  nm) also follow core-shell behavior even at  $R_g/R_{\text{NP}} > 1$ . Figure S5 plots these  $D_{\text{NP}}$  values on a log scale, wherein the data from the different annealing times are easier to distinguish. Figure S5 also includes earlier data from our group studying quantum dots in PPG where  $R_g/R_{\text{NP}} < 1$  and the surface chemistry of the quantum dots was either attractive ( $R_{\text{eff}} = R_{\text{NP}} + R_g$ ) or neutral ( $R_{\text{eff}} = R_{\text{NP}}$ ) toward the PPG. In both cases,  $D_{\text{NP}}$  is well described by  $D_{\text{core-shell}}$ .<sup>25</sup>

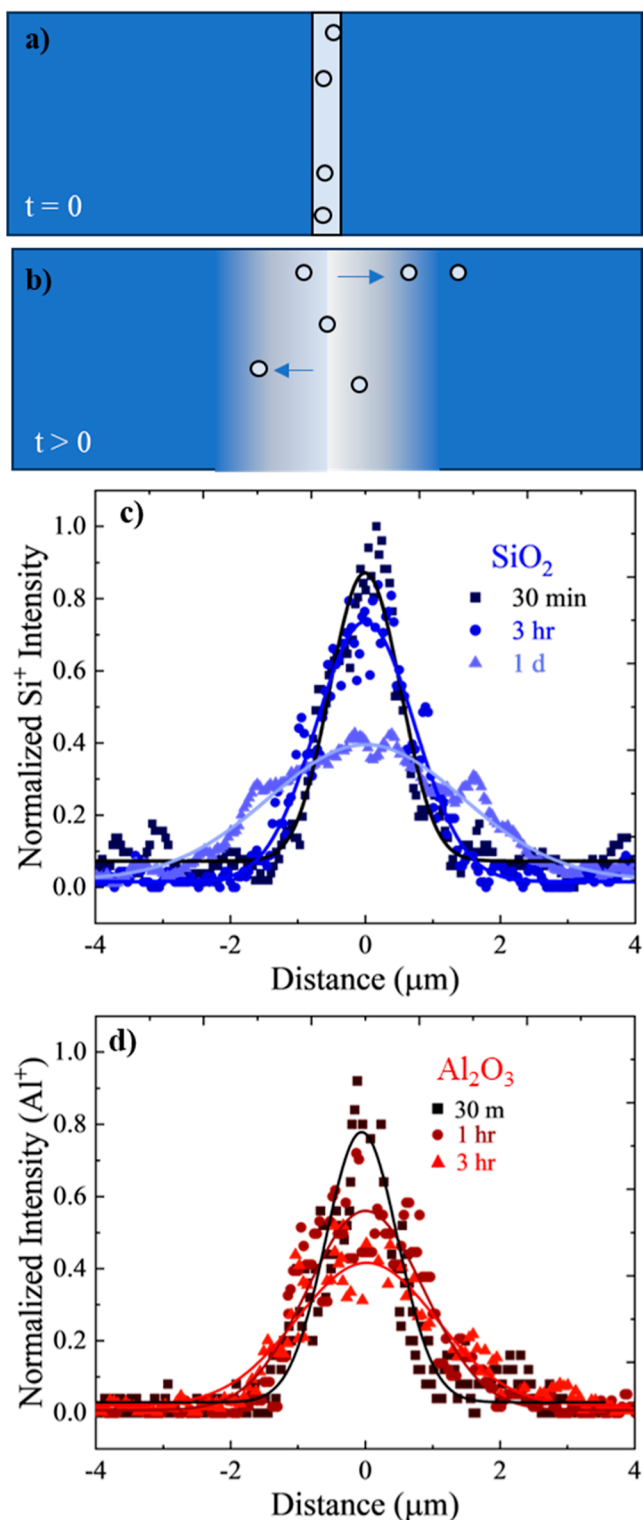


**Figure 1.** (a) Initial sample state at  $t = 0$ , where thick P2VP layers border a thin center PNC layer. (b) Schematic of samples after annealing for a specified time  $t$ . (c) Concentration profiles and fits to eq 6 of  $\text{Si}^+$  signal indicating diffusion of  $\text{SiO}_2$  NPs in 41 kDa P2VP ( $R_g/R_{\text{NP}} = 0.21$ ) at three annealing times. (d) Concentration profiles and fits of integrated  $\text{Al}^+$  data indicating  $\text{Al}_2\text{O}_3$  NP diffusion in 41 kDa P2VP ( $R_g/R_{\text{NP}} = 0.85$ ) at three annealing times.

In contrast, the diffusion coefficient of the  $\text{Al}_2\text{O}_3$  NPs ( $R_{\text{NP}} = 6.5$  nm) significantly deviates from the core-shell mechanism of NP diffusion, Figure 2. While  $D_{\text{NP}}/D_{\text{core-shell}} \approx 1$  when

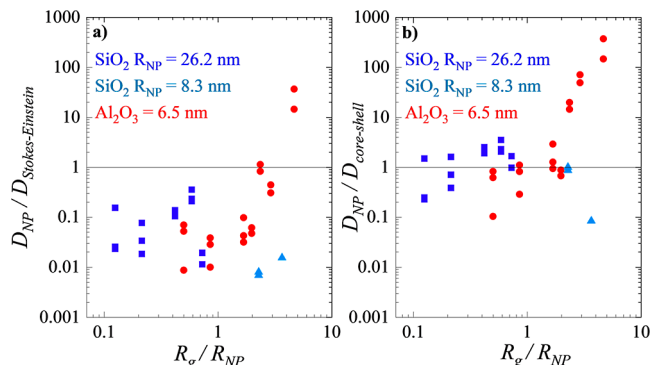


**Figure 2.** NP diffusion coefficients normalized by (a)  $D_{\text{Stokes-Einstein}}$  and (b)  $D_{\text{core-shell}}$  as a function of the polymer  $R_g$  normalized by  $R_{\text{NP}}$ .  $\text{SiO}_2$  NPs are displayed in blue squares ( $R_{\text{NP}} = 26.2$  nm) and light-blue triangles ( $R_{\text{NP}} = 8.3$  nm). Alumina NPs are displayed in red circles ( $R_{\text{NP}} = 6.5$  nm). All annealing times are plotted.

$R_g/R_{\text{NP}} < 1.4$ ,  $D_{\text{NP}}/D_{\text{core-shell}}$  increases dramatically at higher  $R_g/R_{\text{NP}}$ . For example, when the P2VP matrix is  $M_w = 310$  kg/mol and  $R_g/R_{\text{NP}} = 2.4$ ,  $\langle D_{\text{NP}} \rangle / D_{\text{core-shell}}$  is 17 and when the P2VP matrix is  $M_w = 474$  kg/mol and  $R_g/R_{\text{NP}} = 2.9$ ,  $\langle D_{\text{NP}} \rangle / D_{\text{core-shell}}$  is 60. Consequently, we conclude that the  $\text{Al}_2\text{O}_3$  NPs diffuse by a combination of core-shell and vehicular mechanisms. Interestingly, the  $\text{Al}_2\text{O}_3$  NPs exhibit vehicular diffusion while similarly sized  $\text{SiO}_2$  NPs exhibit only core-shell diffusion (see blue triangles at  $R_g/R_{\text{NP}} > 2$ ), which implies that a difference in surface chemistry leads to a faster desorption time for  $\text{Al}_2\text{O}_3$  NPs. In Figure 2b,  $\text{Al}_2\text{O}_3$  NP behavior diverges strongly from  $D_{\text{core-shell}}$  predictions and at  $R_g/R_{\text{NP}} \geq 2.4$ , the discrepancy between  $D_{\text{NP}}$  and  $D_{\text{core-shell}}$  is  $\sim 10^{-14}$   $\text{cm}^2/\text{s}$ , Table S8. Importantly, this difference ( $D_{\text{NP}} - D_{\text{core-shell}}$ ) is nominally independent of molecular weight. Thus, we attribute the faster NP diffusion to the vehicular mechanism given by  $D_{\text{vehicle-II}}$  (eq 4), which is independent of  $M_w$  and has a strong dependence on monomer desorption time,  $\tau_{\text{des}}^{-3/4}$ .

**Monomer Desorption Time of the Bound Layer.** The vehicular and core-shell diffusion mechanisms both contribute to the NP diffusion coefficient ( $D_{\text{NP}}$ ) and are predicated on the existence and lifetime of a bound polymer layer formed through physical adsorption. Core-shell diffusion dominates in systems in which the bound layer is long lived. In contrast, vehicular diffusion occurs in intermediately attractive systems where the rate of stochastic polymer-NP desorption is faster than that observed in the core-shell behavior. An essential facet of vehicular diffusion involves understanding the monomer desorption time ( $\tau_{\text{des}}$ ), a topic not fully explored in nanocomposites with attractive polymer-NP interactions.<sup>17,34</sup> Previous studies of  $\text{SiO}_2$  NPs in P2VP have hinted at a temperature dependence on the bound layer, revealing an effective shell radius and an exchange rate of approximately  $\sim 100$  h.<sup>35</sup> However, factors influencing desorption time, including the polymer-NP interaction strength, molecular weight, entanglement, and NP curvature, remain largely uncharted. This knowledge gap about  $\tau_{\text{des}}$  complicates our grasp of vehicular diffusion, making it challenging to pinpoint the predominant factors influencing fast diffusion. Here, we extract time scales from our prior work to interpret our NP diffusion results, refine our understanding of the vehicular mechanism, and estimate  $\tau_{\text{des}}$  in these PNCs.

To isolate the effect of  $\tau_{\text{des}}$ , we refine eq 1 to account for both NP size and polymer molecular weight and to specify Regime II of the vehicular mechanism

$$D_{\text{NP,theory}}(R_{\text{NP}}, M_w) = D_{\text{core-shell}}(R_{\text{NP}}, M_w) + Ad_T(b^2D_0)^{1/4} \times \left(\frac{1}{\tau_{\text{des}}}\right)^{3/4} \quad (7)$$

Note that Regime I of the vehicular mechanism was dismissed because the NPs in this study have surface hydroxyl groups that have favorable interactions with the nitrogen in P2VP, resulting in slower desorption times. Given  $\tau_e \sim 1$  s and  $D_0 = 1.0 \times 10^{-9}$  cm<sup>2</sup>/s, we estimate  $D_{\text{vehicle-I}} \sim 10^{-9}$  cm<sup>2</sup>/s, which is faster than any of our results even in the lowest  $M_w$ . This is consistent with prior results demonstrating that SiO<sub>2</sub> NPs with hydroxyl surface groups strongly interact with P2VP to have long desorption times.<sup>35–37</sup> Regime III is dismissed because  $D_{\text{vehicle}}$  fails to demonstrate a  $\sim 1/N^{-1/2}$  scaling across  $M_w$  310–474 kDa (eq 5). The molecular weight dependence of  $D_{\text{core-shell}}$  (eq 2) is caused by the molecular weight dependence of  $R_{\text{eff}}$  and  $\eta_{\text{PNC}}$ . The effective NP radius,  $R_{\text{eff}}$ , includes a strongly polymer-bound layer,  $R_{\text{eff}} = R_{\text{NP}} + R_g$  and the molecular weight dependence of  $R_g$  in the melt is well known.<sup>38</sup> The viscosity of the PNC ( $\eta_{\text{PNC}}$ ) is a function of the average volume fraction of the NPs after dilution  $\phi_{\text{NP}}$ , and polymer molecular weight

$$\eta_{\text{PNC}} = \eta_{\text{poly}}(1 + 2.5\phi_{\text{eff}} + 6.2\phi_{\text{eff}}^2) \quad (8)$$

$$\phi_{\text{eff}} = \phi_{\text{NP}} \left(\frac{R_{\text{eff}}}{R_{\text{NP}}}\right)^3 \quad (9)$$

We measured the melt viscosity of the P2VP polymers in this study and fit the data to obtain  $\eta_{\text{poly}}(M_w)$  for eq 8. To capture the Regime II vehicular contribution to  $D_{\text{NP,theory}}$ , we start with the molecular weight dependence of the shortest Rouse time ( $\tau_0$ ) for P2VP as previously measured by broadband dielectric spectroscopy (BDS) at  $T = 413$  K.<sup>13</sup> By assuming a  $1/T$  dependence, we adjust the measured values to temperature of interest  $T = 453$  K (180 °C) and  $\tau_0 \approx 10^{-5}$  s, Figure S6. Then, we compute all relevant time scales by

$$\tau_e = \tau_0 \times N_e^2 \quad (10)$$

$$\tau_{\text{Rouse}} = \tau_0 \times N^2 \quad (11)$$

$$\tau_{\text{rep}} = \tau_{\text{Rouse}} \times \frac{N}{N_e} \quad (12)$$

As previously mentioned, the Al<sub>2</sub>O<sub>3</sub> NPs appear to be in Regime II because the difference between the measured  $D_{\text{NP}}$  and  $D_{\text{core-shell}}$  is independent of the molecular weight. Regime II corresponds to  $\tau_e < \tau_{\text{des}} < \tau_{\text{Rouse}}$ , which for P2VP at 180 °C indicates that  $\tau_{\text{des}}$  is expected to be longer than  $\tau_e \sim 1$  s and shorter than 30–6000 s corresponding to  $\sim 100$ –1220 kDa.

Figure 3a shows the fit of eq 7 to  $D_{\text{NP}}$  for the large SiO<sub>2</sub> NPs as a function of molecular weight. Consistent with Figure 2, the core-shell mechanism is sufficient to describe the NP diffusion of the SiO<sub>2</sub> NPs across all molecular weights. This implies  $D_{\text{vehicle}} \sim 0$ , and therefore  $\tau_{\text{des}} (>6000$  s) is exceedingly large and consistent with a highly attractive P2VP–SiO<sub>2</sub> interaction. Figure 3b shows the experimental data for the Al<sub>2</sub>O<sub>3</sub> NPs along

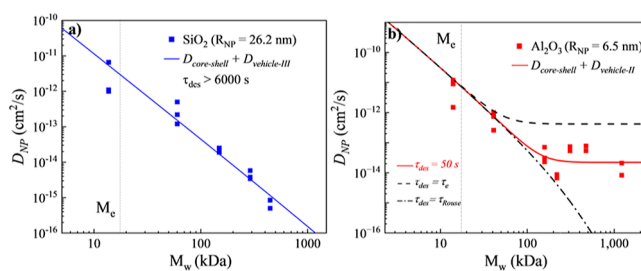


**Figure 3.** (a)  $D_{\text{NP}}$  (blue points) for SiO<sub>2</sub> (26.2 nm) NPs in P2VP as a function of molecular weight. Solid line corresponds to  $D_{\text{theory}}$  in eq 7 where  $D_{\text{vehicle}} \rightarrow 0$  as  $\tau_{\text{des}} \gg \tau_{\text{Rouse}}$ . (b)  $D_{\text{NP}}$  (red points) for Al<sub>2</sub>O<sub>3</sub> (6.5 nm) NPs in P2VP as a function of molecular weight. Red line is the best fit to eq 7 and corresponds to  $\tau_{\text{des}} = 50$  s. Black dashed and dot-dash lines correspond to  $\tau_{\text{des}} = \tau_e$  and  $\tau_{\text{des}} = \tau_{\text{Rouse}}$  respectively.

with the fit to eq 7 using  $A = 1$ ,  $d_T = 23.5$  nm,  $b = 1.8$  nm, and  $D_0 = 1.0 \times 10^{-9}$  cm<sup>2</sup>/s.<sup>13</sup> The best fit corresponds to  $\tau_{\text{des}} = 50$  s, which falls within the bounds established above. To illustrate the bounds corresponding to Regime II of vehicular NP diffusion, we plot eq 7 using the  $\tau_{\text{des}} = \tau_e$ , which is independent of  $M_w$  and  $\tau_{\text{des}} = \tau_{\text{Rouse}}$ , which increases with  $M_w$ . These upper and lower limits of  $D_{\text{NP}}$  for the Al<sub>2</sub>O<sub>3</sub> NPs in P2VP further confirm that this system is in Regime II at 180 °C.

These results indicate that NP diffusion coefficients can provide valuable insights into the monomer desorption times and polymer–NP interactions. Given the core–shell behavior of small SiO<sub>2</sub> NPs (Figure 2) and the vehicular mechanism found in Al<sub>2</sub>O<sub>3</sub> NPs of similar size, our results show that Al<sub>2</sub>O<sub>3</sub> NPs exhibit weaker polymer–NP interactions. This finding is consistent with water contact angle measurements for silica ( $\sim 80^\circ$ ) and alumina ( $\sim 90^\circ$ ) that suggest a lower areal density of hydroxyl groups on alumina leading to weaker interactions consistent with a short  $\tau_{\text{des}}$ .<sup>39,40</sup> Additionally, poly(vinylpyrrolidone) (PVP) preferentially adsorbs to unmodified silica particles over alumina-coated counterparts in aqueous solution, and the preadsorbed PVP transfers from the alumina-coated particles to silica particles as the system equilibrates. Adsorption isotherms further demonstrate that PVP adhesion to silica particles is stronger than to alumina-coated silica particles, which demonstrates that the silica particle surface is more polar.<sup>41</sup> This result is consistent with our finding that the monomeric desorption time of P2VP is longer for silica NPs than for alumina NPs. Overall, this study establishes that both the relative size of the polymer to the NP ( $R_g/R_{\text{NP}}$ ) and the polymer–NP interfacial interactions dictate the transition for NP diffusion from solely a core–shell behavior mechanism to the addition of vehicular mechanisms. Further investigations could explore various methods for controlling polymer–NP interactions, including using random copolymers, as well as the effect of NP shape on diffusion.

## CONCLUSIONS

We experimentally demonstrate both core–shell and vehicle mechanisms for NP diffusion in polymer melts. While large and small silica NPs demonstrate the core–shell mechanism (eq 2) due to highly attractive polymer–NP interactions and long monomer desorption times,  $\tau_{\text{des}}$ , small alumina NPs display a crossover from core–shell to vehicular NP diffusion. For the Al<sub>2</sub>O<sub>3</sub> NPs,  $D_{\text{NP}}$  exhibits a plateau as  $M_w$  increases and  $R_g > R_{\text{NP}}$ , and this molecular weight independent behavior is consistent with Regime II of the vehicular mechanism. At high  $M_w$ , the Al<sub>2</sub>O<sub>3</sub> NP diffusion coefficients are one or two orders of

magnitude faster than that predicted by the core–shell model alone. Fitting the data reveals a  $\tau_{\text{des}}$  of  $\sim 50$  s that is independent of  $M_w$  and indicates a weaker polymer–NP interaction in P2VP/Al<sub>2</sub>O<sub>3</sub> than in P2VP/SiO<sub>2</sub> nanocomposites. We have demonstrated that by measuring NP diffusion coefficients in polymer melts, one can determine the polymer–NP interaction strengths, which have previously been difficult to ascertain. This study provides a pathway to measure monomer desorption times ( $\tau_{\text{des}}$ ) for a variety of PNC systems to explore the role of temperature, NP size, NP surface functionality, and polymer composition to understand the lifetime of the polymer-bound layer on NPs. We found that the core–shell and vehicle diffusion modes apply broadly to entangled melts with attractive polymer–NP interactions.

## ■ ASSOCIATED CONTENT

### SI Supporting Information

The Supporting Information is available free of charge at <https://pubs.acs.org/doi/10.1021/acs.macromol.4c00808>.

Molecular weight characterization of P2VP and calculated  $R_g$ , spin-coating conditions to create P2VP films, spin-coating conditions to create polymer nanocomposite films, ToF SIMS mass spectra distinguished  $m/q = 27$  (Al<sup>+</sup>) and  $m/q = 28$  (Si<sup>+</sup>) peaks, normalized concentration profiles from ToF SIM for SiO<sub>2</sub> NPs ( $R_{\text{NP}} = 26.2$  nm) diffusing into P2VP ( $M_w = 14.0$ – $474$  kDa), normalized concentration profiles from ToF SIM for Al<sub>2</sub>O<sub>3</sub> NPs ( $R_{\text{NP}} = 6.5$  nm) diffusing into P2VP ( $M_w = 14.0$ – $1220$  kDa), normalized concentration profiles from ToF SIM for SiO<sub>2</sub> NPs ( $R_{\text{NP}} = 8.3$  nm) diffusing into P2VP ( $M_w = 474$  and  $1220$  kDa), measured diffusion coefficients for large SiO<sub>2</sub> ( $R_{\text{NP}} = 26.2$  nm) in P2VP ( $14.0$ – $474$  kDa), measured diffusion coefficients for small Al<sub>2</sub>O<sub>3</sub> ( $R_{\text{NP}} = 6.5$  nm) in P2VP ( $14.0$ – $1220$  kDa), measured diffusion coefficients for small SiO<sub>2</sub> ( $R_{\text{NP}} = 8.3$  nm) in P2VP ( $474$  and  $1220$  kDa), nanoparticle diffusion coefficients from the core–shell model ( $D_{\text{core-shell}}$ ) at  $T = 180$  °C as a function of molecular weight,  $D_{\text{NP}}/D_{\text{core-shell}}$  vs  $R_g/R_{\text{NP}}$  showing data from all annealing times, evidence for Regime II vehicular diffusion, and shortest Rouse time ( $\tau_0$ ) for P2VP measured at  $140$  °C and scaled to  $180$  °C (PDF)

## ■ AUTHOR INFORMATION

### Corresponding Author

Karen I. Winey – Department of Materials Science and Engineering, University of Pennsylvania, Philadelphia, Pennsylvania 19104, United States; Department of Chemical and Biomolecular Engineering, University of Pennsylvania, Philadelphia, Pennsylvania 19104, United States; [orcid.org/0000-0001-5856-3410](https://orcid.org/0000-0001-5856-3410); Email: [winey@seas.upenn.edu](mailto:winey@seas.upenn.edu)

### Author

Kaitlin Wang – Department of Materials Science and Engineering, University of Pennsylvania, Philadelphia, Pennsylvania 19104, United States; [orcid.org/0000-0003-2459-8767](https://orcid.org/0000-0003-2459-8767)

Complete contact information is available at: <https://pubs.acs.org/10.1021/acs.macromol.4c00808>

## Notes

The authors declare no competing financial interest.

## ■ ACKNOWLEDGMENTS

We acknowledge funding from NSF CBET 2034122. We thank Dr. Jamie Ford at the Singh Center for Nanotechnology at the University of Pennsylvania for his expertise regarding ToF-SIMS, supported by NSF-MRSEC-DMR-2309043. We thank Roshni John Chethalen at the University of Massachusetts Amherst for providing GPC analysis. We thank Ravisara Wattana at the University of Pennsylvania for providing viscosity characterization of P2VP. We thank Dr. Eric Bailey and Dr. Will Drayer for insightful discussion.

## ■ REFERENCES

- (1) Kumar, S. K.; Benicewicz, B. C.; Vaia, R. A.; Winey, K. I. 50th Anniversary Perspective: Are Polymer Nanocomposites Practical for Applications? *Macromolecules* **2017**, *50*, 714–731.
- (2) Méar, F.; Coillot, D.; Podor, R.; Montagne, L. Self-Healing Nanocomposites: Role and Activation of Inorganic Moieties and Hybrid Nanophases. *Self-Healing at the Nanoscale*; CRC Press, 2011; pp 188–223.
- (3) Mallakpour, S.; Naghdi, M. Polymer/SiO<sub>2</sub> nanocomposites: Production and applications. *Prog. Mater. Sci.* **2018**, *97*, 409–447.
- (4) Thakur, V. K.; Kessler, M. R. Self-Healing Polymer Nanocomposite Materials: A Review. *Polymer* **2015**, *69*, 369–383.
- (5) Young, W. W.; Katsumata, R. Intermediate Polymer Relaxation Explains the Anomalous Rheology of Nanocomposites with Ultra-small Attractive POSS Nanoparticles. *ACS Polym. Au* **2023**, *3*, 466–474.
- (6) Merkel, T. C.; Freeman, B. D.; Spontak, R. J.; He, Z.; Pinnau, I.; Meakin, P.; Hill, A. J. Ultraporous, Reverse-Selective Nanocomposite Membranes. *Science* **2002**, *296*, 519–522.
- (7) Yin, J.; Deng, B. Polymer-Matrix Nanocomposite Membranes for Water Treatment. *J. Membr. Sci.* **2015**, *479*, 256–275.
- (8) Cheng, S.; Xie, S.-J.; Carrillo, J.-M. Y.; Carroll, B.; Martin, H.; Cao, P.-F.; Dadmun, M. D.; Sumpter, B. G.; Novikov, V. N.; Schweizer, K. S.; Sokolov, A. P. Big Effect of Small Nanoparticles: A Shift in Paradigm for Polymer Nanocomposites. *ACS Nano* **2017**, *11*, 752–759.
- (9) Balazs, A. C.; Emrick, T.; Russell, T. P. Nanoparticle Polymer Composites: Where Two Small Worlds Meet. *Science* **2006**, *314*, 1107–1110.
- (10) Lin, C.-C.; Parrish, E.; Composto, R. J. Macromolecule and Particle Dynamics in Confined Media. *Macromolecules* **2016**, *49*, 5755–5772.
- (11) Cheng, S.; Holt, A. P.; Wang, H.; Fan, F.; Bocharova, V.; Martin, H.; Etampawala, T.; White, B. T.; Saito, T.; Kang, N.-G.; Dadmun, M. D.; Mays, J. W.; Sokolov, A. P. Unexpected Molecular Weight Effect in Polymer Nanocomposites. *Phys. Rev. Lett.* **2016**, *116*, 038302.
- (12) Papakonstantopoulos, G. J.; Yoshimoto, K.; Doxastakis, M.; Nealey, P. F.; De Pablo, J. J. Local Mechanical Properties of Polymeric Nanocomposites. *Phys. Rev. E: Stat., Nonlinear, Soft Matter Phys.* **2005**, *72*, 031801–031806.
- (13) Bailey, E. J.; Griffin, P. J.; Composto, R. J.; Winey, K. I. Multiscale Dynamics of Small, Attractive Nanoparticles and Entangled Polymers in Polymer Nanocomposites. *Macromolecules* **2019**, *52*, 2181–2188.
- (14) Griffin, P. J.; Bocharova, V.; Middleton, L. R.; Composto, R. J.; Clarke, N.; Schweizer, K. S.; Winey, K. I. Influence of the Bound Polymer Layer on Nanoparticle Diffusion in Polymer Melts. *ACS Macro Lett.* **2016**, *5*, 1141–1145.
- (15) Cheng, S.; Carroll, B.; Bocharova, V.; Carrillo, J.-M.; Sumpter, B. G.; Sokolov, A. P.; Carrillo, J.-M. Y. Focus: Structure and dynamics of the interfacial layer in polymer nanocomposites with attractive interactions. *J. Chem. Phys.* **2017**, *146*, 203201.

- (16) Yamamoto, U.; Carrillo, J.-M. Y.; Bocharova, V.; Sokolov, A. P.; Sumpter, B. G.; Schweizer, K. S. Theory and Simulation of Attractive Nanoparticle Transport in Polymer Melts. *Macromolecules* **2018**, *51*, 2258–2267.
- (17) Carroll, B.; Bocharova, V.; Carrillo, J.-M. Y.; Kisliuk, A.; Cheng, S.; Yamamoto, U.; Schweizer, K. S.; Sumpter, B. G.; Sokolov, A. P. Diffusion of Sticky Nanoparticles in a Polymer Melt: Crossover from Suppressed to Enhanced Transport. *Macromolecules* **2018**, *51*, 2268–2275.
- (18) Tuteja, A.; Mackay, M. E.; Narayanan, S.; Asokan, S.; Wong, M. S. Breakdown of the Continuum Stokes-Einstein Relation for Nanoparticle Diffusion. *Nano Lett.* **2007**, *7*, 1276–1281.
- (19) Lin, C.-C.; Gam, S.; Meth, J. S.; Clarke, N.; Winey, K. I.; Composto, R. J. Do Attractive Polymer–Nanoparticle Interactions Retard Polymer Diffusion in Nanocomposites? *Macromolecules* **2013**, *46*, 4502–4509.
- (20) Liu, J.; Cao, D.; Zhang, L. Molecular Dynamics Study on Nanoparticle Diffusion in Polymer Melts: A Test of the Stokes-Einstein Law. *J. Phys. Chem. C* **2008**, *112*, 6653–6661.
- (21) Grabowski, C. A.; Mukhopadhyay, A. Size Effect of Nanoparticle Diffusion in a Polymer Melt. *Macromolecules* **2014**, *47*, 7238–7242.
- (22) Cai, L. H.; Panyukov, S.; Rubinstein, M. Hopping Diffusion of Nanoparticles in Polymer Matrices. *Macromolecules* **2015**, *48*, 847–862.
- (23) Cai, L.-H.; Panyukov, S.; Rubinstein, M. Mobility of Nonsticky Nanoparticles in Polymer Liquids. *Macromolecules* **2011**, *44*, 7853–7863.
- (24) Cole, D. H.; Shull, K. R.; Rehn, L. E.; Baldo, P. M. RBS Analysis of the Diffusion of Nano-Size Spheres in a Polymer Matrix. *Nucl. Instrum. Methods Phys. Res., Sect. B* **1998**, *136–138*, 283–289.
- (25) Park, J.; Bailey, E. J.; Composto, R. J.; Winey, K. I. Single-Particle Tracking of Nonsticky and Sticky Nanoparticles in Polymer Melts. *Macromolecules* **2020**, *53*, 3933–3939.
- (26) Mendez, N. F.; Dhara, D.; Zhang, Q.; Narayanan, S.; Schadler, L. S.; Müller, A. J.; Kumar, S. K. Nanoparticle Diffusion in Miscible Polymer Nanocomposite Melts. *Macromolecules* **2023**, *56*, 4658–4668.
- (27) Kwon, N. K.; Park, C. S.; Lee, C. H.; Kim, Y. S.; Zukoski, C. F.; Kim, S. Y. Tunable Nanoparticle Stability in Concentrated Polymer Solutions On the Basis of the Temperature Dependent Solvent Quality. *Macromolecules* **2016**, *49*, 2307.
- (28) Wang, K.; Composto, R. J.; Winey, K. I. ToF-SIMS Depth Profiling to Measure Nanoparticle and Polymer Diffusion in Polymer Melts. *Macromolecules* **2023**, *56*, 2277–2285.
- (29) Spool, A. M. *The Practice of TOF-SIMS: Time of Flight Secondary Ion Mass Spectrometry*—Alan M. Spool—Google Books; Momentum Press, 2016.
- (30) Mei, H.; Laws, T. S.; Terlier, T.; Verduzco, R.; Stein, G. E. Characterization of Polymeric Surfaces and Interfaces Using Time-of-Flight Secondary Ion Mass Spectrometry. *Polym. Sci.* **2021**, *60*, 1174–1198.
- (31) Prasad, A.; Salim, N. V.; Mozetič, M.; Kailas, L.; Thomas, S. Time-of-flight Secondary Ion Mass Spectrometric Analysis of Polymer Surfaces: A Review. *J. Appl. Polym. Sci.* **2022**, *139*, 52286.
- (32) Karar, N.; Gupta, T. K. Study of Polymers and Their Blends Using TOF-SIMS Ion Imaging. *Vacuum* **2015**, *111*, 119–123.
- (33) Chan, C. M.; Weng, L. T. Surface Characterization of Polymer Blends by XPS and ToF-SIMS. *Materials* **2016**, *9*, 655.
- (34) Ge, T. Scaling Perspective on Dynamics of Nanoparticles in Polymers: Length- and Time-Scale Dependent Nanoparticle-Polymer Coupling. *Macromolecules* **2023**, *56*, 3809–3837.
- (35) Jimenez, A. M.; Zhao, D.; Misquitta, K.; Jestin, J.; Kumar, S. K. Exchange Lifetimes of the Bound Polymer Layer on Silica Nanoparticles. *ACS Macro Lett.* **2019**, *8*, 166–171.
- (36) Bailey, E. J.; Griffin, P. J.; Composto, R. J.; Winey, K. I. Characterizing the Areal Density and Desorption Kinetics of Physically Adsorbed Polymer in Polymer Nanocomposite Melts. *Macromolecules* **2020**, *53*, 2744–2753.
- (37) Harton, S. E.; Kumar, S. K.; Yang, H.; Koga, T.; Hicks, K.; Lee, H.; Mijovic, J.; Liu, M.; Vallery, R. S.; Gidley, D. W. Immobilized Polymer Layers on Spherical Nanoparticles. *Macromolecules* **2010**, *43*, 3415–3421.
- (38) Rubinstein, M.; Colby, R. H. *Polymer Physics*; Oxford University Press, 2003.
- (39) Jin, J.; Wang, X.; Wick, C. D.; Dang, L. X.; Miller, J. D. Silica Surface States and Their Wetting Characteristics. *Surf. Innovations* **2020**, *8*, 145–157.
- (40) Watcharenwong, A.; Saijaiou, N.; Bailuang, Y.; Kajitvichyanukul, P. Morphology and Wettability of Nanoporous Aluminium Oxide Film Prepared by Anodization. *Key Eng. Mater.* **2017**, *737*, 174–178.
- (41) Cooper, C. L.; Cosgrove, T.; Van Duijneveldt, J. S.; Murray, M.; Prescott, S. W. Colloidal Particles in Competition for Stabilizer: A Solvent Relaxation NMR Study of Polymer Adsorption and Desorption. *Langmuir* **2012**, *28*, 16588–16595.